ISSN 0021-3640, JETP Letters, 2023, Vol. 117, No. 11, pp. 814–820. © The Author(s), 2023. This article is an open access publication.
Russian Text © The Author(s), 2023, published in Pis'ma v Zhurnal Eksperimental'noi i Teoreticheskoi Fiziki, 2023, Vol. 117, No. 11, pp. 819–825.

OPTICS
AND LASER PHYSICS

Random Laser Based on Materials in the Form of Complex Network Structures

A. Yu. Bazhenov[a], M. M. Nikitina[a], D. V. Tsarev[a], and A. P. Alodjants[a, *]

[a] *ITMO University, St. Petersburg, 197101 Russia*

**e-mail: alexander_ap@list.ru*

Received April 18, 2023; revised April 22, 2023; accepted April 22, 2023

The theory of a random laser with an interface in the form of random or scale-free networks whose nodes are occupied by microcavities with quantum two-level systems has been proposed for the first time. The microcavities are coupled to each other through light-guiding channels forming edges of the network. It has been shown that such a laser has a number of spectral features associated with the statistical properties of the network structure. Among them are the existence of a topologically protected Perron eigenvalue caused by the presence of a strong mean field at the node of maximum influence located in the central part of the network and the delocalization/localization of radiation modes depending on the probability of coupling between arbitrary microcavities. The results obtained in this work open prospects for the fabrication of new low-threshold laser sources.

DOI: 10.1134/S0021364023601264

Random lasers are among the most fascinating manifestation of macroscopic coherence caused by the random scattering of light in a disordered optically active medium [1]. The main physical principles of the operation of modern random lasers were proposed by V.S. Letokhov for atomic systems [2]. These principles are continuously extended and refined taking into account the variety of media where the random laser effect is observed [1, 3–5]. Since such lasers do not require external cavities, their properties are determined by the intensity of radiation scattering in the medium. The weak scattering of photons by particles of the medium forms the diffusive random laser regime, whereas strong scattering leads to the Anderson localization of radiation [3]. These key properties make random lasers practically useful.

However, the effect of the disorder of the medium on random laser regimes has yet to be studied (see [6]). The authors of [4] implemented a random laser based on a structure of nanofibers forming a random graph, which were placed in the rhodamine 6G dye responsible for the gain of radiation. Our analysis [7, 8] of the formation of macroscopically coherent radiation in complex network structures showed that the lasing threshold decreases rapidly with an increase in the connectivity of the graph simulating the medium, which was detected experimentally for random lasers in [4]. It is noteworthy that the investigation of such complex network structures is one of the most interesting and important fields of modern physics and has a pronounced interdisciplinary significance [9].

The aim of this work is to reveal the mechanism of lasing in the medium with the topology of a random (Fig. 1a) or scale-free (Fig. 1b) undirected graph formed by coupled microcavities.

The system under consideration can be represented as a network with nodes where two-level systems, e.g., quantum dots, are located. This can be achieved, e.g., as in [5] by placing two-level systems in a photon-crystal structure with channels for the propagation of photons. Alternatively, two-level systems can be placed in microcavities, which are physically coupled micropillars [10]. To be more specific, in this work, we use the model of coupled microcavities (see [11]). Thus, the random laser model consists of N microcavities each containing the same two-level system characterized by a resonance transition frequency (energy) of ω_0. Microcavities are located at nodes of the complex network with the edges transmitting light without loss. The field in the ith microcavity is characterized by the photon annihilation (creation) operator $\hat{f}_i$ ($\hat{f}_i^\dagger$), $i = 1,\ldots,N$. The Hamiltonian of the system in the rotating wave approximation can be represented in the form [12]

$$\hat{H} = \hbar\sum_{i=1}^{N}\left[\frac{\omega_0\hat{\sigma}_i^z}{2} + \omega_{\mathrm{ph},i}\hat{f}_i^\dagger\hat{f}_i + g(\hat{f}_i\hat{\sigma}_i^+ + \hat{f}_i^\dagger\hat{\sigma}_i^-)\right] - \frac{\hbar J}{2}\sum_{i,j=1}^{N}\tau_{ij}(\hat{f}_j^\dagger\hat{f}_i + \hat{f}_i^\dagger\hat{f}_j), \quad (1)$$

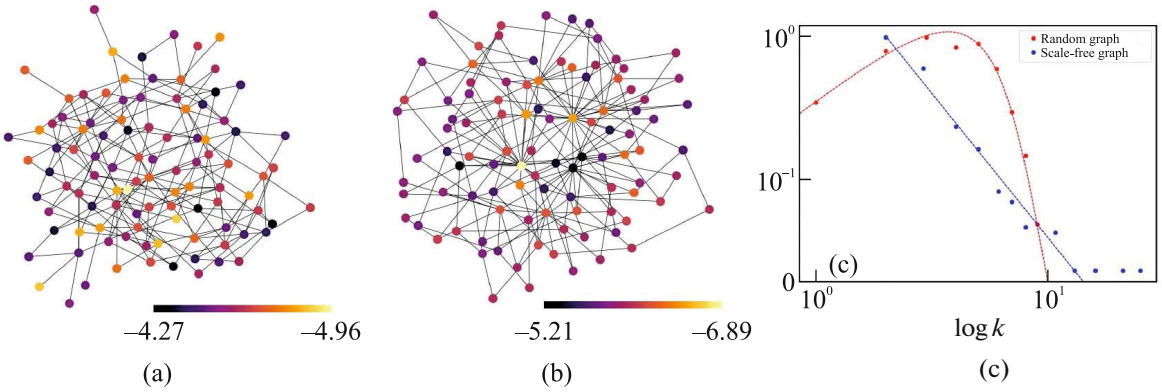

Fig. 1. (Color online) Interface of the random laser medium in the form of the (a) random ($k_{max} = 9$ and $k_{min} = 1$) and (b) scale-free ($k_{max} = 25$ and $k_{min} = 2$) networks at $N = 100$; $k_{max/min}$ is the maximum/minimum degree of nodes. Colors characterize the eigenvalues of the adjacency matrix τ_{ij}. (c) Log–log distribution of degrees of nodes of the corresponding networks. The other details are presented in the main text.

where the two-level system in the ith microcavity is characterized by the inversion operator $\hat{\sigma}_i^z$ and ladder operators $\hat{\sigma}_i^{\pm}$; g is the coupling constant of the two-level system with a quantum field mode in the ith microcavity at the frequency $\omega_{ph,i}$; $J > 0$ specifies the interaction between microcavities through waveguides (photon channels), which is included through the symmetric adjacency matrix τ_{ij} with zero diagonal elements; and p_{ij} is the probability of coupling between the ith and jth microcavities (if the ith and jth microcavities with $i \neq j$ are coupled, $\tau_{ij} = 1$).

Figure 1 presents the interface of the random lasers in the form of the Erdős–Rényi random network (Fig. 1a) and scale-free network (Fig. 1b), which were simulated numerically using the Python NetworkX library. The sets of points and approximating curves in Fig. 1c are log–log distribution functions of degrees of nodes of these networks. Curves correspond to the Poisson ($p_k = \frac{1}{k!}\langle k\rangle^k e^{-\langle k\rangle}$) and power-law ($p_k \propto k^{-\eta}$) distributions, where $\langle k\rangle = \frac{1}{N}\sum_j k_j = \frac{1}{N}\sum_{i,j}\tau_{ij}$ is the average degree of nodes. The simulation parameters were chosen such that both graphs in Fig. 1 have similar statistical characteristics. In particular, $\langle k\rangle = 4.04$ and $\zeta = 4.88$ for the random network, where $\zeta \equiv \sum_i k_i^2/N\langle k\rangle$ is the normalized second moment of the degrees of nodes. The degree η for the scale-free network and its statistical properties can be estimated in the continuous approximation using approaches presented in [9]; setting $k_{max} = k_{min}N^{\frac{1}{\eta-1}}$, we obtain $\eta \simeq 2.82$ and, correspondingly, $\langle k\rangle = 3.9$ and $\zeta = 6.1$. The scale-free network has hubs, i.e., nodes with the highest connectivity indicated by four blue points for the distribution function in the lower right corner of Fig. 1c.

We used the Heisenberg–Langevin approach in the mean field approximation; taking into account Eq. (1), this approach leads to Maxwell–Bloch-type equations:

$$\dot{\mathcal{E}}_i = (-i\omega_{ph,i} - \kappa_i)\mathcal{E}_i - ig\bar{P}_i + iJ\sum_j \tau_{ij}\mathcal{E}_j; \quad (2a)$$

$$\dot{\bar{P}}_i = (-i\omega_0 - \Gamma)\bar{P}_i + ig\sigma_i^z\mathcal{E}_i; \quad (2b)$$

$$\dot{\sigma}_i^z = (\gamma_P - \gamma_D) - (\gamma_P + \gamma_D)\sigma_i^z + 2ig(\mathcal{E}_i^*\bar{P}_i - \mathcal{E}_i\bar{P}_i^*), \quad (2c)$$

where $\mathcal{E}_i = \langle\hat{f}_i\rangle$, $\bar{P}_i = \langle\hat{\sigma}_i^-\rangle$, and $\sigma_i^z = \langle\hat{\sigma}_i^z\rangle$ are the means of the corresponding operators; Γ is the polarization relaxation rate, which is taken the same for all two-level systems; κ_i is the rate of losses of photons in the ith microcavity; γ_P is the pumping rate; and γ_D is the inversion relaxation rate. Further, we exclude "fast" oscillations and consider steady states of the system at the frequency ω. The substitution of $\bar{P}_i(t) = P_i e^{-i\omega_0 t - i\omega t}$ and $\mathcal{E}_i(t) = E_i e^{-i\omega_0 t - i\omega t}$ into Eqs. (2a) and (2b) gives

$$(\omega - \Delta_i + i\kappa_i)E_i - gP_i + J\sum_{j=1}^{N}\tau_{ij}E_j = 0; \quad (3a)$$

$$(i\Gamma + \omega)P_i + g\sigma_i^z E_i = 0, \quad (3b)$$

where $\Delta_i = \omega_{ph,i} - \omega_0$ is the detuning from resonance for the ith microcavity, which is assumed to be quite small $|\Delta_i| < g$ for all $i = 1,\ldots,N$. The average population inversion in Eq. (2c) is given such that $\dot{\sigma}_i^z = 0$ and $\sigma_i^z \simeq \frac{\gamma_P - \gamma_D}{\gamma_P + \gamma_D}$ (cf. [6]).

The value $\omega = 0$ in Eqs. (3a) and (3b) physically means the evolution of both the (mean) field and the

polarization at the frequency ω_0 of the transition in two-level systems.

The substitution of the polarization P_i expressed from Eq. (3b) into Eq. (3a) yields the following equation for the complex field amplitude E_i in the ith microcavity:

$$\left\{(\omega - \Delta_i + i\kappa_i)\omega_\Gamma + \sigma^z\right\} E_i + J\omega_\Gamma \sum_{j=1}^{N} \tau_{ij} E_j = 0, \quad (4)$$

where $\omega_\Gamma \equiv \omega + i\Gamma$ and the parameters ω, Δ_i, κ_i, Γ, and J are normalized to g.

We now analyze an important limiting case of (4), where the ith microcavity is isolated from the remaining network structure. In this case, $\tau_{ij} = 0$ in Eq. (4), and we obtain the expressions

$$\omega_{1,2} = -i\chi_{+,i} + \frac{1}{2}(\Delta_i \pm \sqrt{(\Delta_i - 2i\chi_{-,i})^2 - 4\sigma^z}), \quad (5)$$

which determine the characteristic high- (ω_1) and low-frequency (ω_2) elementary oscillations, where $\chi_{\pm,i} \equiv (\kappa_i \pm \Gamma)/2$. A negative imaginary part of the frequency $\mathrm{Im}[\omega] < 0$ in Eq. (5) describes energy dissipation in the system, whereas $\mathrm{Im}[\omega] > 0$ corresponds to inversion-induced gain. In particular, in the inversion-free case, i.e., at $\sigma^z \simeq -1$, the characteristic frequencies ω_1 and ω_2 correspond to conventional polaritons of the upper and lower dispersion branches, respectively [13]. At the maximum inversion $\sigma^z \simeq 1$, Raman polaritons appear, corresponding to the gain of radiation in the medium [14]. Further, conditions for the transition of the considered system of microcavities to lasing when $0 \le \sigma^z \le 1$ are of interest. For numerical calculations, it is convenient to use the initial system of Eqs. (3a) and (3b) under the assumption that the detuning Δ_i and the parameter κ_i for any ith mode of the random laser are random variables uniformly distributed in certain intervals (cf. [6]).

Figure 2 presents the dependences of the imaginary parts of the eigenfrequencies of the random laser on their real parts that are slightly below the lasing threshold determined by the condition $\mathrm{Im}[\omega] = 0$ and correspond to the graphs in Fig. 1. In agreement with expectations, two regions of solutions are formed, corresponding to the characteristic frequencies ω_1 and ω_2. The numerical values of the parameters κ_i/g and Γ/g for the dependences in Fig. 2 and below in the paper were chosen such that the condition of strong coupling between each two-level system and the field, $\kappa_i, \Gamma < 1$, is satisfied hardly (cf. [10]).

We analyze the arrangement of points in Fig. 2. Since both graphs in Fig. 1 have close statistical characteristics $\langle k\rangle$ and ζ, the "envelopes" of the discrete dependences presented in Fig. 2 are fairly close to each other. A fundamental feature of the spectrum of eigen-

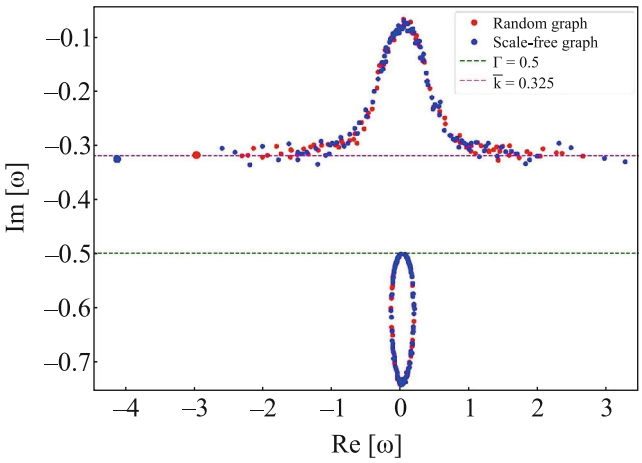

Fig. 2. (Color online) Eigenfrequencies of the random lasers on the complex ω plane for the (red circles) random and (blue circles) scale-free networks presented in Fig. 1 at $\sigma^z = 0.1$, $\Gamma = 0.5$, and $J = 0.6$; Δ_i and κ_i are the random variables uniformly distributed in the intervals [–0.5,0.5] and [0.5Γ,0.8Γ], respectively.

frequencies is the existence of the isolated (maximum in absolute value) Perron eigenvalue (the leftmost red and blue points in Fig. 2). This is directly due to the properties of the spectrum of the adjacency matrix τ_{ij} for complex networks for which the Perron eigenvalue is in the interval $[\langle k\rangle, k_{\max}]$ (see, e.g., [15]). Light yellow nodes located approximately in the centers of graphs in Figs. 1a and 1b correspond to the Perron eigenvalues. In particular, the Perron–Frobenius theorem guarantees (for τ_{ij}) the existence of the nondegenerate positive maximum Perron eigenvalue corresponding to the eigenvector with completely positive elements; since Eq. (1) includes $-\tau_{ij}$, the corresponding Perron eigenvalues in Fig. 2 are negative.

We note that the Perron eigenvalue does not necessarily correspond to a hub, i.e., a node with the highest connectivity. The Perron eigenvalue characterizes the node of maximum influence determined by the eigenvector centrality criterion [16]. For example, random networks do not have hubs but have the node of maximum influence indicated by the light yellow point in Fig. 1a. The existence of such nodes is physically due to a nonzero average (over nodes of the network) field

$$\bar{E} = \frac{1}{N\langle k\rangle} \sum_{j=1}^{N} k_j E_j, \quad (6)$$

where $k_j = \sum_i \tau_{ij}$ is the degree of the jth node.

To study the Perron eigenvalue, we substitute the annealed network approximation for the adjacency matrix in the form $\tau_{ij} = \dfrac{k_i k_j}{N\langle k\rangle}$ (cf. [7, 9]) into Eq. (4).

Solving the resulting equation with respect to E_i, we obtain

$$E_i = -\frac{J(\omega_P + i\Gamma)k_i\overline{E}}{\left\{(\omega_P - \Delta_i + i\overline{\kappa})(\omega_P + i\Gamma) + \sigma^z\right\}}, \quad (7)$$

where $\overline{\kappa}$ is the average loss of photons in a given interval of κ_i and ω_P is the Perron eigenvalue for the frequency. Expression (7) means that the field at the ith node corresponding to the Perron eigenvalue is completely determined by the mean field $\overline{E}$ induced by the network structure. Substituting Eq. (7) into Eq. (6), we obtain an equation for ω_P, from which

$$\mathrm{Re}[\omega_{P,1}] \simeq -J\zeta, \quad \mathrm{Im}[\omega_{P,1}] \simeq -\overline{\kappa}, \quad (8a)$$

$$\mathrm{Re}[\omega_{P,2}] = 0, \quad \mathrm{Im}[\omega_{P,2}] = -\Gamma, \quad (8b)$$

where we omit the detuning Δ_j assuming that $\Delta_j \ll J\zeta$ and consider the simple case $\sigma^z \simeq 0$. Formulas (8a) and (8b) are in agreement with the numerical simulation (see Fig. 2, where $\mathrm{Im}[\omega_{P,1}]$ is shown by the pink dashed line). The characteristic low frequency $\omega_{P,2}$ remains imaginary: $\mathrm{Im}[\omega_{P,2}]$ is given by the green dashed line in Fig. 2, which physically means the fast dissipation of low-frequency perturbations in the presence of high-frequency oscillations at the frequency of the Perron eigenvalue $\mathrm{Re}[\omega_{P,1}]$. We note that, since the parameter ζ for the scale-free network is larger in absolute value than that for the random network (cf. [7]), the Perron eigenvalue in the former case (thick blue point) is to the left of the Perron eigenvalue for the random network marked by the bold thick red point in Fig. 2.

We now consider points in Fig. 2 that are located along the line of average loss of photons $\mathrm{Im}[\omega] = -\overline{\kappa}$ and for which $E_i \simeq E_j$. This assumption is justified because of the properties of the adjacency matrix, which has a relatively large Perron eigenvalue and other smaller eigenvalues (see [15]). This group includes both points with significant influence and hubs existing in the scale-free network (see Fig. 1b). As a result, from Eq. (4), the characteristic frequencies are

$$\omega_{1,2} = -i\chi_+ + \frac{1}{2}(\delta_i \pm \sqrt{(\delta_i - 2i\chi_-)^2 - 4\sigma^z}), \quad (9)$$

where $\chi_\pm \equiv (\overline{\kappa} \pm \Gamma)/2$ and $\delta_i \equiv \Delta_i - Jk_i$ is the detuning from resonance also including the degree k_i of the ith node. It is convenient to perform the subsequent analysis of the discussed points in the limit $|\delta_i| \simeq Jk_i \gg \sqrt{(\kappa_i - \Gamma)^2 + 4\sigma^z}$, i.e., under the assumption that Jk_i is large enough. Then, it follows from Eq. (9) that (cf. Eq. (8))

$$\mathrm{Re}[\omega_1] \simeq -Jk_i + \frac{\sigma^z}{Jk_i}, \quad \mathrm{Im}[\omega_1] \simeq -\overline{\kappa}, \quad (10a)$$

$$\mathrm{Re}[\omega_2] \simeq -\frac{\sigma^z}{Jk_i}, \quad \mathrm{Im}[\omega_2] \simeq -\Gamma, \quad (10b)$$

which are in good agreement with the numerical calculation shown in Fig. 2. In this case, the spread of positive eigenfrequencies along the horizontal axis is larger for the scale-free network because the rightmost blue points correspond to hubs.

We now consider the points in Fig. 2 located in a relatively narrow vertical band $-1 < \mathrm{Re}[\omega] < 1$. These points include two groups that are closely located in the upper and lower parts of Fig. 2 and correspond to the main set of the eigenvalues of the system of Eqs. (3a) and (3b) and to the eigenvalues of the adjacency matrix τ_{ij} (cf. [15]). A fundamental feature of these points is that eigenvalues corresponding to these points can "attract" each other because the (random) matrix corresponding to the system of Eqs. (3a) and (3b) is non-Hermitian (cf. [17]). More precisely, we deal here with the non-Hermitian localization of radiation significantly different from (Hermitian) Anderson localization, which is manifested in the statistical properties of spectral characteristics (see, e.g., [18]). Such (non-Hermitian) localization significantly affects the statistical distribution of spectral lines: the deviation of this distribution from the Wigner distribution of distances between levels, which is characteristic of Anderson localization, was demonstrated in the experiment with the random laser (see [4, 19]).

The modes corresponding to the points in the upper part of Fig. 2 first tend to enter the half-plane, where lasing occurs; i.e., $\mathrm{Im}[\omega] > 0$. Their "mobility" is due to their topological correspondence to nodes with a small number of links or low-influence nodes located predominantly at the periphery of graphs (see Fig. 1), which is also confirmed by experimental results obtained for lasing in random lasers on graphs [4].

To determine the characteristic frequencies corresponding to the points grouped near $\omega = 0$, Eq. (9) can be used under the assumption that $\delta_i \simeq \Delta_i - Jk_{\min}$ is small, where $k_{\min}$ is the minimum degree of nodes in the graph. The numerical simulation shows that lasing begins when points in the upper part of Fig. 2 enter the half-plane of real eigenvalues, which is described by the condition

$$\sigma^z \simeq \overline{\kappa}\Gamma + \frac{\delta_i^2}{4}. \quad (11)$$

If $|\delta_i|\chi_-, \delta_i^2, \chi_-^2 \ll 1$, from Eqs. (9) and (11), we obtain

$$\mathrm{Re}[\omega_{1,2}] \simeq \frac{\delta_i}{2}, \quad \mathrm{Im}[\omega_1] = 0, \quad \mathrm{Im}[\omega_2] \simeq -2\chi_+; \quad (12)$$

i.e., the frequency ω_1 becomes real. In this limit, the last term in Eq. (11) can be neglected and the lasing condition takes a form very universal for laser physics (cf. [20]).

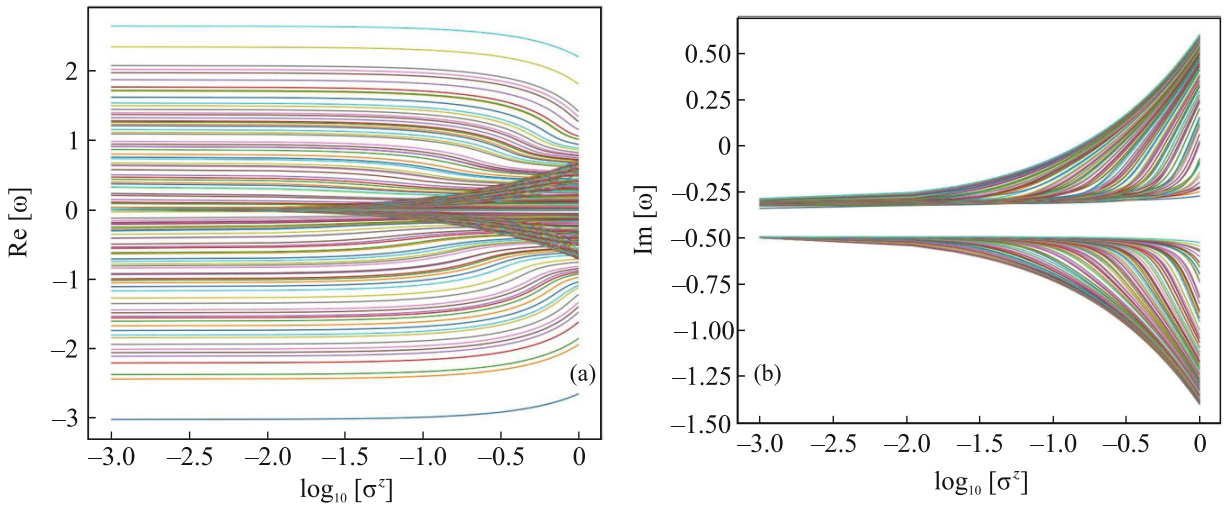

Fig. 3. (Color online) (a) Real and (b) imaginary parts of the eigenfrequencies of the random laser, which is a random graph, versus the common logarithm of the population difference σ^z. The remaining parameters are the same as in Fig. 2.

Figure 3 presents the dependences of $\mathrm{Re}[\omega]$ and $\mathrm{Im}[\omega]$ for the random laser on the logarithm of the population inversion σ^z. It is seen in Fig. 3a that points located in the band $-1 < \mathrm{Re}[\omega] < 1$ are displaced with increasing inversion σ^z. The eigenfrequencies corresponding to this group of points in Fig. 3a approach each other, which characterizes the pulling of the lasing frequency to the transition frequency in the two-level system ω_0 (in this case, $\omega \simeq 0$, cf. [6]).

At the same time, the bottom (blue) line in Fig. 3a corresponding to the frequency of the Perron eigenvalue $\mathrm{Re}[\omega_{\mathrm{P},\,1}]$ changes slightly with increasing σ^z. A similar behavior is shown by the blue and yellow lines in the upper part of Fig. 3a, which correspond to the rightmost points in Fig. 2 and to nodes having significant influence in the random network next after the Perron eigenvalue (cf. Fig. 1a). Thus, microcavities located at the nodes of maximum influence remain topologically protected and are hardly involved in the frequency pulling process; the imaginary parts of the corresponding eigenfrequencies do not enter the gain region $\mathrm{Im}[\omega] > 0$ (see Fig. 3b).

The asymptotic behavior of lines in Fig. 3b above the lasing threshold can be clarified as follows. Let the two-level system be completely inverted; i.e., $\sigma^z \simeq 1$. In this case, under the assumption that $|\delta_i^2 - 4\chi_-^2| \ll 4$ in Eq. (9), we obtain $\delta_i^2 - 4 - 4\chi_-^2 < 0$. Separating the real and imaginary parts in Eq. (9) (see, e.g., [13]), we obtain $\mathrm{Im}[\omega_1] = 1 - \chi_+ \simeq 0.59$ and $\mathrm{Im}[\omega_2] = -(1 + \chi_+) \simeq -1.41$, which are in good agreement with the maximum and minimum values of the extreme lines in Fig. 3b at $\log \sigma^z = 0$, respectively.

The characteristic dependences of the real and imaginary parts of the frequency ω on the population difference in the scale-free network (Fig. 1a) are similar to those in Fig. 3. Significant differences between these dependences appear when the distribution of degrees of nodes has a power-law form $p_k \propto k^{-\eta}$ with the exponent $1 < \eta < 2.5$ (cf. [7]). The role of hubs in this network increases strongly, which is manifested in their spectral characteristics: hubs begin to compete with the Perron eigenvalue in "influence" on the network. In this case, according to the numerical calculation, it is reasonable to take into account correlations between nodes with degrees higher than ζ (cf. Eq. (8a)). This limit will be analyzed elsewhere.

Finally, in the context of the physics of random lasers, it is necessary to pay attention to the behavior of the effective volume of modes defined as (cf. [6])

$$V_j = \sum_{i=1}^{N} \frac{1}{\max\limits_i [|E_{i,j}|^2]} |E_{i,j}|^2, \qquad (13)$$

where $E_{i,j}$ is the field amplitude in the ith cavity for the jth eigenvector of the system of Eqs. (3a) and (3b).

The effect of the statistical properties of the random network on the localization of states in the considered problem is demonstrated in Fig. 4. This figure presents the dependence of the average volume V filled by the jth mode of the random laser averaged over a large number of realizations of random graphs on the probability $p = p_{ij}$ of connection between each pair of N nodes. In this case, the average degree of nodes is $\langle k \rangle = p(N-1) \simeq pN$ [9]. The dependence in Fig. 4 was calculated beginning with the value $p = 0.01$ corresponding to $\langle k \rangle \simeq 1$.

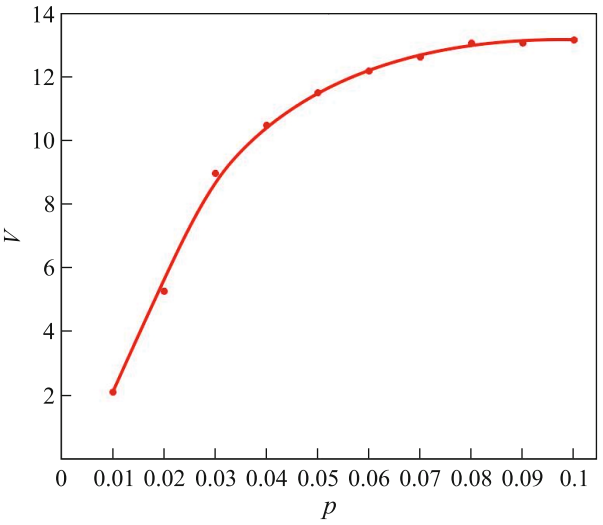

Fig. 4. (Color online) Average volume of modes V of the random laser averaged over a large number of realizations of random graphs versus the probability p; points are obtained numerically, and the solid line is their approximation. The remaining parameters are the same as in Fig. 2.

The random network in the region $0 < \langle k \rangle < 1$ consists of separate microcavities weakly coupled to each other; as a result, calculated fluctuations of the volume of modes are large; the minimum value of any mode is unity at its complete localization, according to definition (13).

The degree of connectivity of the random graph increases with p (and, correspondingly, with $\langle k \rangle$). The value $p = 0.1$ in Fig. 4 corresponds to $\langle k \rangle \simeq 10$, at which the graph already has a giant (connected) component. Thus, the increase in the average volume with the average degree of nodes $\langle k \rangle$ indicates the transition from localized states (at $\langle k \rangle < 1$) to the delocalization of radiation inherent in a random graph with a giant connected component. The saturation of the corresponding curve is due to the disappearance of isolated nodes in the random graph, which occurs in the limit $\langle k \rangle \gg 1$ (see Fig. 4).

We note that the numerical calculation shows that the behavior of the average volume of modes V (i.e., the localization/delocalization of radiation) for the random laser considered in this work as a function of other material parameters of the random laser (e.g., population inversion) can differ from the behavior of "conventional" random lasers demonstrating the almost exponential delocalization of radiation in their structure [6]. In our case, this effect depends not only on the statistical properties of the graph (adjacency matrix) but also on the characteristic parameters of the decoherence, dissipation, and detuning from resonance (cf. [17]). In the general case, the investigation of the localization/delocalization of radiation for various combinations of these parameters is a very interesting and nontrivial (at least, theoretically) problem, which we will consider elsewhere.

To summarize, we have studied the model of coupled microcavities, which contain two-level systems and are located at nodes of the complex (random or scale-free) network whose edges are light-guiding channels coupling these microcavities. The system under consideration demonstrates the main properties of random lasers including both localization and delocalization of light depending on the statistical properties of the network structure. In this aspect, the proposed model of random laser is in qualitative agreement with recent experiments with the random laser formed by a random network of nanofibers. At the same time, the considered model of laser has a quite interesting spectral property: the (isolated) Perron eigenvalue maximal in absolute value exists for frequencies because different nodes make different contributions to lasing (statistical properties of the degrees of different nodes are different). We are going to examine these problems for a wider range of the material parameters of the laser than the range studied in this work.

FUNDING

This work was supported by the Russian Science Foundation (project no. 23-22-00058 "Coherent Effects in Two-Dimensional Quantum Materials with the Complex Network Interface").

CONFLICT OF INTEREST

The authors declare that they have no conflicts of interest.

OPEN ACCESS

REFERENCES

1. D. Wiersma and S. Diederik, Nat. Phys. **4**, 359 (2008).
2. V. S. Letokhov, Sov. Phys. JETP **26**, 835 (1967).

3. C. Hui, Y. Xu Junying, L. Yong, A. L. Burin, E. W. Seeling, X. Liu, and R. P. H. Chang, IEEE J. Sel. Top. Quantum Electron. **9**, 111 (2003).
4. M. Gaio, D. Saxena, J. Bertolotti, D. Pisignano, A. Camposeo, and R. Sapienza, Nat. Commun. **10**, 226 (2019).
5. L. Sapienza, H. Thyrrestrup, S. Stobbe, P. D. Garcia, S. Smolka, and P. Lodahl, Science (Washington, DC, U. S.) **327**, 1352 (2010).
6. Yu. V. Yuanov, A. A. Zyablovsky, E. S. Andrianov, I. V. Doronin, A. A. Pukhov, A. P. Vinogradov, and A. A. Lisyansky, JETP Lett. **112**, 688 (2020).
7. A. Yu. Bazhenov, M. M. Nikitina, and A. P. Alodjants, JETP Lett. **115**, 644 (2022).
8. A. P. Alodjants, A. Yu. Bazhenov, A. Y. Khrennikov, and A. V. Bukhanovsky, Sci. Rep. **12**, 8566 (2022).
9. A.-L. Barabási, *Network Science* (Cambridge Univ. Press, Cambridge, 2016).
10. A. Dousse, J. Suffczyński, R. Braive, A. Miard, A. Lemaître, I. Sagnes, L. Lanco, J. Bloch, P. Voisin, and P. Senellart, Appl. Phys. Lett. **94**, 121102 (2009).
11. I.-H. Chen, Y. Y. Lin, Y.-C. Lai, E. S. Sedov, A. P. Alodjants, S. M. Arakelian, and R.-K. Lee, Phys. Rev. A **86**, 023829 (2012).
12. A. Halu, S. Garnerone, A. Vezzani, and G. Bianconi, Phys. Rev. E **87**, 022104 (2013).
13. S. Pau, G. Björk, J. Jacobson, Hui Cao, and Y. Yamamoto, Phys. Rev. B **51**, 14437 (1995).
14. A. Y. Bazhenov, D. V. Tsarev, and A. P. Alodjants, Phys. B: Condens. Matter **579**, 411879 (2020).
15. C. Sarkar and S. Jalan, Chaos **28**, 102101 (2018).
16. M. E. J. Newman, in *The New Palgrave Dictionary of Economics* (Palgrave Macmillan, London, 2018), p. 8525.
17. J. Feinberg and A. Zee, Phys. Rev. E **59**, 6433 (1999).
18. M. Sade, T. Kalisky, S. Havlin, and R. Berkovits, Phys. Rev. E **72**, 066123 (2005).
19. G. M. Zaslavskii, Sov. Phys. Usp. **22**, 788 (1979).
20. H. Haken, *Light,* Vol. 2: *Laser Light Dynamics* (North-Holland, Amsterdam, 1981).

Translated by R. Tyapaev